Measurement of the V2I Channel in Cell-free Vehicular Networks with the Distributed MaMIMOSA Channel Sounder

Eric Pierre Simon*, Pierre Laly*, Joumana Farah†, Emmeric Tanghe‡, Wout Joseph‡, Davy Paul Gaillot*
*University of Lille, CNRS, UMR 8520 - IEMN Lille, eric.simon@univ-lille.fr
†Univ Rennes, INSA Rennes, CNRS, IETR-UMR 6164, F-35000 Rennes, France
‡Department of Information Technology, IMEC-WAVES, Ghent University, Belgium

***Abstract*—In this paper, we present a small, yet realistic, vehicular cell-free massive MIMO (multiple-input multiple-output) architecture deployed at the University of Lille in a typical suburban environment under both Line-of-Sight (LOS) and obstructed LOS (OLOS) shadowing conditions. The radio channels were acquired with a distributed RF-over-Fiber (RoF) upgrade of the real-time channel sounder MaMIMOSA. The system operates at 5.89 GHz with an 80 MHz bandwidth, which corresponds to the ITS frequency band offered by the ITS-G5 and C-V2X technologies. Four omnidirectional receive antennas were placed on the roof of a van moving at a speed of 25 km/h. The propagation channel was measured for various transmit antenna configurations, ranging from co-located antennas to fully distributed antennas. The measurement results show a significant gain in the signal-to-noise ratio (SNR) as well as a more uniform coverage and smaller delay spread values with the distributed scenarios compared to the centralized ones. Finally, the path loss measurement results obtained for the cell-free network provide deployment guidelines for the distributed antennas.**

***Index Terms*—cell-free, MIMO, channel sounding.**

I. Introduction

5G mobile networks are currently built according to a cell architecture with a base station (BS) at its center. The BS is equipped with an array of many antennas called massive multiple-input multiple-output (MIMO) which is one of many cornerstones of the 5G technology. The benefits of massive MIMO are numerous and have been widely studied in the literature [1]. However, 5G networks still suffer from the limitations attributed to their inherent cellular architecture. On the one hand, there is an extreme variation in the received power level between the center and edge of the cell. This results in a substantial variation in the signal-to-noise-ratio (SNR) and, therefore, quality of service (QoS). On the other hand, users located at the cell-edge suffer from interference from neighboring cells. Hence, a cellular architecture is not compatible to meet the challenges of future wireless communications applications and provide ubiquitous wireless connectivity.

A new network architecture without the concept of cells appeared a few years ago: the cell-free mobile network [2], [3], [4], [5]. In the cell-free context, an important number of access points (APs) distributed over a large geographical area cooperate to optimally serve the users (UE). These APs are equipped with a small number of antennas and are connected to a central processing unit (CPU) via a wired or wireless backhaul link. The cell-free concept encompasses the 5G massive MIMO technique wherein many antennas are densely distributed over the area. As a result, cell-free massive MIMO can be viewed as a generalization of 5G massive MIMO. Due to the proximity and diversity of APs, it offers a far more uniform coverage and increased connectivity. In particular, critical life-safety services considered in upcoming vehicular networks specifically rely on a highly uniform QoS.

Although the cell-free massive MIMO has recently received a lot of attention at the theoretical level, there is only one recent experimental study in the literature that investigates the attractive features of *vehicular* cell-free massive MIMO [6]. In that work, the topology under investigation consisted in distributing 32 transmit (Tx) antennas along an axis of 46.5 m on a building rooftop with different configurations. In contrast, in this paper, it is considered that the antennas are fully deployed over the area of interest at the street level, as imagined for road-side units (RSU) with V2I applications. Furthermore, different possible Tx antenna system topologies are investigated, i.e. the number of APs and antennas per AP altogether with their locations. Indeed, recent articles showed that the semi-distributed multi-antenna APs is the best configuration [7], [8], [9] from system-level performance perspective. Nonetheless, these results are solely based on an indoor measured massive MIMO dataset. Hence, the validation of this approach for outdoor vehicular applications is simply missing in the literature. To tackle vehicular networks, the real-time channel sounder MaMIMOSA has been upgraded to measure channels in such distributed configurations. Initially, MaMIMOSA was jointly developed by the University of Lille (France) and Ghent (Belgium) to measure co-located massive MIMO channels for vehicular scenarios [10]. In particular, it was recently set up to measure the time-varying 64×16 radio channel at 5.89 GHz with an 80 MHz bandwidth. The upgrade consists in geographically distributing the transmit antennas using up to 500 meter-long RF-over-fiber (RoF) links. This enables the real-time channel between a vehicle and a network of distributed antennas to be measured. The current MaMIMOSA configuration supports up to 8 single-antenna APs or L APs equipped each with a N-antenna

array, with $L \times N = 8$. Based on the measurements, the performance of the different topologies are compared in terms of the achievable mean SNR, delay spread, and path loss characteristics.

II. Distributed MaMIMOSA

The propagation channels are measured with the MaMIMOSA radio channel sounder [11], [12]. Data are modulated using orthogonal frequency-division multiplexing (OFDM) with 8192 subcarriers using a 12.21 kHz subcarrier spacing. The streaming mode of MaMIMOSA is selected for the vehicular context. It corresponds to the frame structure illustrated in Fig. 1. Each frame is emitted every 510 ms and starts with a 51.2 µs preamble, followed by 4096 OFDM symbols. This yields a duration of around 500 ms. Each Tx antenna transmits a pilot every eight sub-carriers, with one sub-carrier per antenna shift to interleave the Tx antenna signals. Note that one OFDM symbol out of 32 was recorded for this campaign. The purpose of this work does not include a complete Doppler analysis due to the lack of space but this will be addressed in subsequent work.

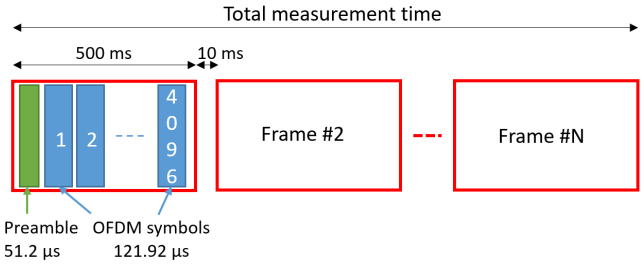

Fig. 1. MaMIMOSA Streamshot Frame structure

For the time being, eight 500 meter-long RoF links with 1 dB/km attenuation loss are connected to MaMIMOSA and TX as shown in Fig. 2. The RF-optical converters integrate a power amplifier to compensate for the insertion losses at the expense of a 27 dB noise figure. The output power was set to 0 dBm for each RF chain and a 15 dB gain power amplifier was placed in between the optical/RF module and antenna to reach a 15 dBm transmit power signal with 40 dB SNR. The length of all coaxial cables was 2.5 m. A hybrid calibration procedure using one of the RoF links was performed since both RoF and coaxial links are used.

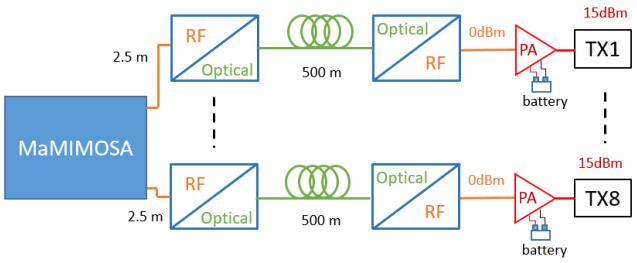

Fig. 2. Cell-free sounding architecture using 8 RoF links and one coaxial link

III. Measurement campaign description

The channel measurement campaign took place on the Cité Scientifique Campus of the University of Lille (France). A picture of the MaMIMOSA transmission system, playing the role of the cell-free CPU, is shown in Fig 3. 6.5 dBi patch antennas were used at the transmitting APs (Fig. 4). The receiver was a van equipped with four 2 dBi EM6116 omnidirectional antennas on its rooftop spaced apart by more than 10λ (i.e. more than 0.5 m with $\lambda \sim 5.1$ cm) to ensure a decorrelated reception, as illustrated in Fig. 5. The receiving (Rx) MaMIMOSA system was carried inside the van. Both Tx and Rx units were powered with Li-ion batteries that provide up to 8 hours of continuous measurements.

Fig. 3. MaMIMOSA transmission system with the 500m long RoF links

The measurement scenario consisted in driving the van on a section of the campus boulevard from point A to point B over a 275 m distance with a roundabout in-between at an average speed of 25 km/h (Fig. 6). Four AP configurations were investigated in this campaign from fully co-located to fully distributed antennas. The first one consists in one AP equipped with 8 antennas, the second one 2 APs equipped with 4 antennas each, the third one 4 APs equipped with 2 antennas each, and the fourth one 8 single-antenna APs. These configurations are called Config. 1 to 4 throughout the text, respectively. The deployment of the APs is shown in Fig. 6, where each position has been numbered. The orientation of the Tx patch antennas is depicted by an arrow pointing toward the emission direction. The Tx antennas are positioned at a height of 2.5 m and are vertically polarized. The mean distances between APs are around 225 m, 85 m, and 40 m for the Config. 2, 3, and 4, respectively.

For each transmission configuration, the radio channel was measured with the streaming mode using $\sim$ 70 frames giving a complete recording of $\sim$ 35 seconds.

IV. Measurement results

First, the SNR values are estimated for each Tx - Rx link as a function of time. Then, the obtained SNRs are averaged over the four Rx antennas for each Tx.

Fig. 4. Setup of the investigated linear array configurations with 1, 2, and 8 patch antennas per AP. The red box indicates a 4-antenna AP as a subset of the 8-antenna AP

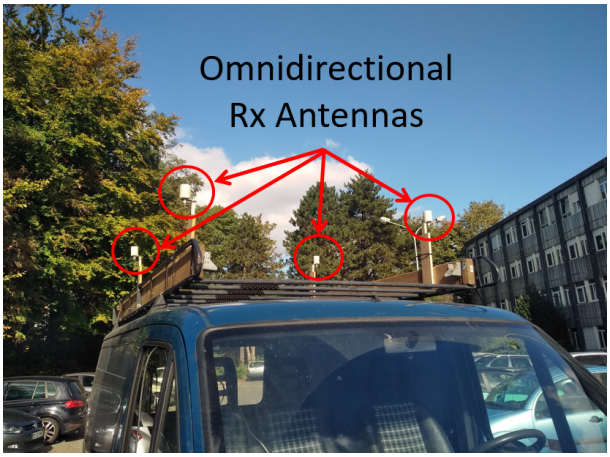

Fig. 5. MaMIMOSA Omnidirectional Rx antennas

Fig. 7 shows, for each configuration, the maximum SNR obtained among the eight Tx antennas. In practice, this would be equivalent to an antenna selection criterion based on the SNR. This choice is motivated to reduce the implementation cost by limiting the system to a unique radio-frequency (RF) chain. The results clearly demonstrate the efficiency of distributing the Tx antennas over the coverage area. Indeed, for Config. 1, the reception quality starting from A is observed to be rather poor since Rx is relatively far from Tx. Quality is only improved when Rx gets nearer to the end of its path (i.e. point B) and, therefore, closer to Tx. This proves that the receiver does not always benefit from the multi-antenna diversity due to

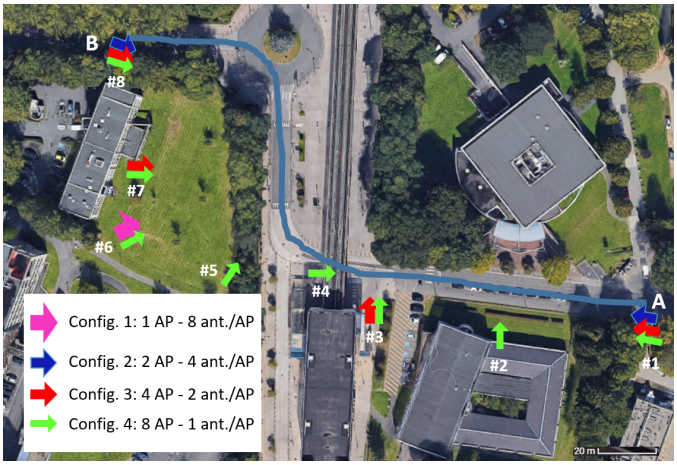

Fig. 6. Top-view of the measurement campaign on the Lille University Cité Scientifique Campus presenting the four AP configurations

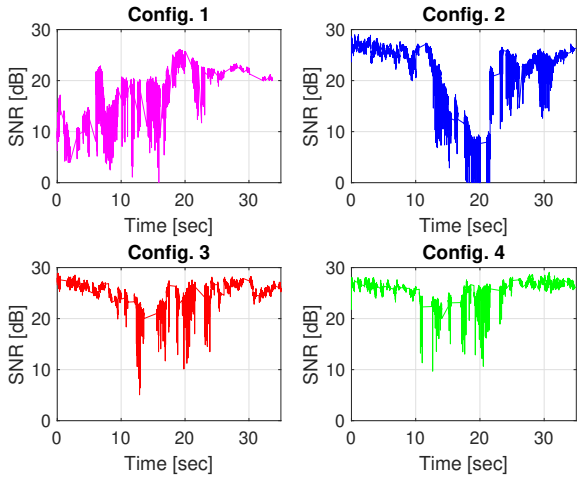

Fig. 7. SNR for the four AP configurations

distance and blockage by vegetation and obstacles. In Config. 2, the two APs with four antennas are positioned near points A and B, respectively. This explains the important drop in SNR for a significant duration around the middle of the trip. The minimum SNR level in Config. 1 and Config. 2 is nearly 0 dB, whereas it is much larger for Config. 3 and Config. 4 with 5 dB and 10 dB, respectively. The decrease in SNR near the area of dense vegetation (around the middle of the path) is still noticeable in the last two configurations but is alleviated by the distribution of the antennas. In any configuration, the SNR values are typically large when a LOS exists (typically above 20 dB) and smaller for OLOS conditions (due to the vegetation). From this point of view, displacing (or adding) an AP to the other side of the road would have been greatly beneficial to the reception quality.

Fig. 8 shows the corresponding cumulative distribution function (CDF). The advantages of Config. 3 and 4 are highlighted compared to the other two. Nearly 49% (resp.

80%) of the van positions present an SNR higher than 20 dB in Config. 1 (resp. Config. 2) compared to 98.5% and nearly 100% in Config. 3 and Config. 4.

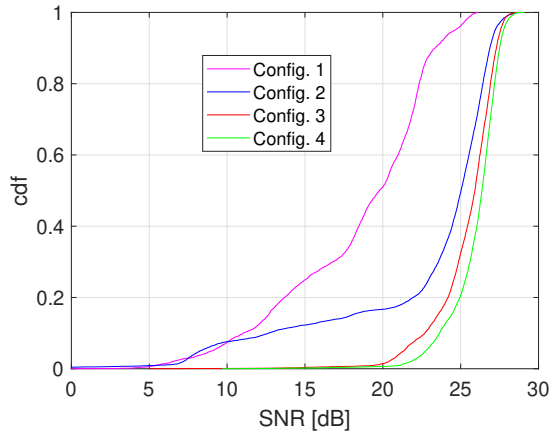

Fig. 8. CDF of the SNR for the four AP configurations

Moreover, still considering the aforementioned antenna selection criterion, the channel root mean square (RMS) delay spread was computed for the first Rx and the best corresponding Tx (see Fig. 9). Only the van positions that yield an SNR higher than a threshold of 10 dB are considered. The delay spread values are found to be varying between 12.5 (minimum measurable rms) to 150 ns and are in line with values reported in the literature for a similar scenario and shadowing conditions (see [13] for example). It is noticed that distributing the antennas allows a higher number of van positions with low RMS delay spread values. These low values generally correspond to LOS links between transmit and receive antennas, which are more frequent in distributed scenarios. This effect is further confirmed in Fig. 10 which shows the corresponding CDF. The results show a clear advantage of the three distributed configurations with respect to the centralized Config. 1, while the other three exhibit a similar behavior in terms of RMS delay spread.

To further investigate these results, Fig. 11 presents, for each configuration, the CDF of the RMS delay spread of the link corresponding to the first Rx and:

- the Tx yielding the maximum RMS delay spread (dashed lines),
- the Tx yielding the minimum RMS delay spread (dotted lines),
- the Tx yielding the highest SNR (solid lines).

A first observation is that distributing the antennas (ex: Config. 4) naturally produces higher values of the maximum RMS delay spread, compared to less distributed configurations. However, the minimum RMS delay spread is the smallest for Config. 4. Additionally, our antenna selection criterion based on SNR yields very close RMS delay spread values to those obtained with a decision based on the observed RMS delay spread.

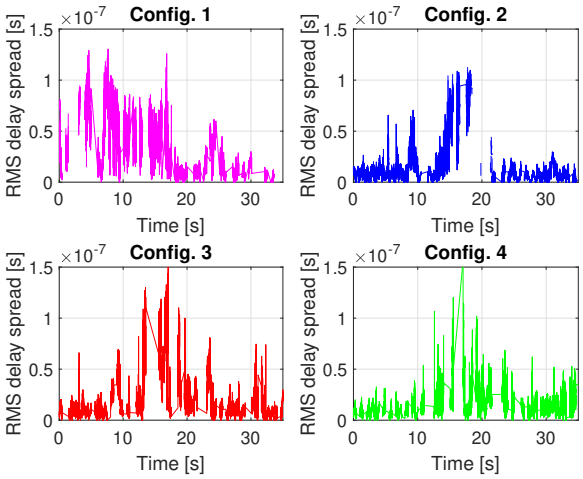

Fig. 9. RMS delay spread for the four AP configurations

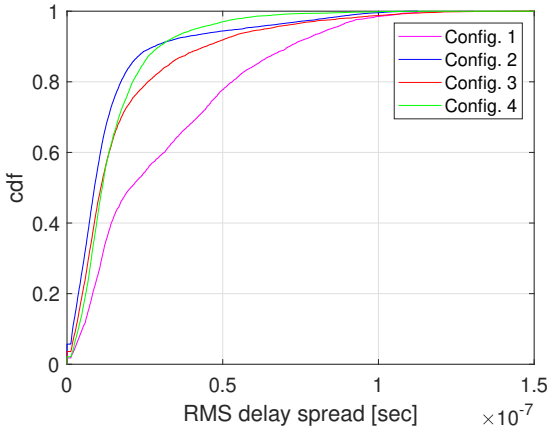

Fig. 10. CDF of the RMS delay spread for the four AP configurations

Optimized deployment strategies of the distributed cell-free network are currently missing in the literature for a realistic complex propagation scenario. Here, the dependence of the AP location in the scenario on the propagation fading properties was investigated for the fully distributed Config. 4. This analysis is critical as it provides some guidelines to distribute the APs with respect to the foliage, buildings, and the AP antenna orientation with respect to the receivers. To this end, the path loss exponent n and lognormal shadow fading χ_g were derived for each AP location from the received gain averaged across the receivers, when driving from B to A. Since the receiver crosses the AP during the drive-test, the analysis was split into two datasets (a) and (b). (a) corresponds to the trip from B to the AP, whereas (b) corresponds to the trip from the AP to A. AP locations 5 to 7 were omitted because the corresponding datasets were not of sufficient quality to compute the path loss characteristics. The results presented in Table I indicate that n varies between 1.85 and 4.89, with the χ_g values being below 3 dB, which are in line with values

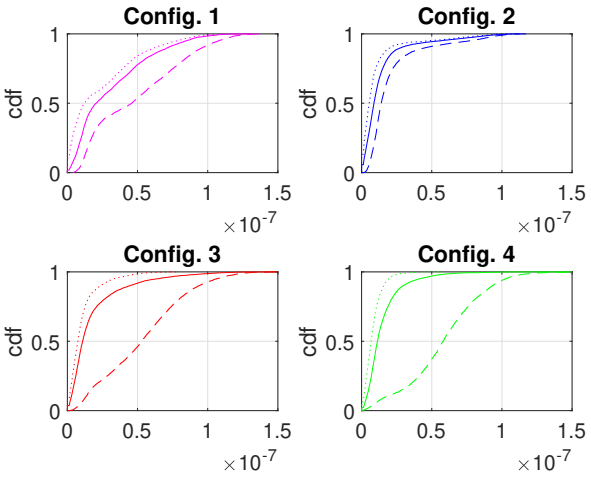

Fig. 11. CDF of the maximum (dashed line), minimum (dotted line) and highest SNR (solid line) RMS delay spread for the four AP configurations

obtained in similar scenarios. It is shown that the links with a strong LOS (i.e. AP1, AP2(b), AP4(b), and AP8) exhibit n values close to 2 (free space propagation). In contrast, for the other OLOS shadowing conditions, larger n values are obtained. AP2(a) has the largest value of n because there is the presence of a building element that obscures the LOS as the vehicle approaches the antenna.

TABLE I
PATH LOSS CHARACTERISTICS BETWEEN EACH AP OF THE FULLY DISTRIBUTED CONFIG. 4 AND RECEIVER

AP	n	χ_g (dB)
1	1.98	1.75
2(a)	4.89	2.5
2(b)	1.90	1.26
3(a)	2.62	1.59
3(b)	2.81	1.38
4(a)	3.92	1.91
4(b)	2.01	2.04
8	1.85	2.23

V. CONCLUSION

For the first time to our knowledge, this paper deals with radio channel measurements in a realistic vehicular cell-free network. The measurements were performed with an 80 MHz bandwidth at 5.89 GHz using an upgraded version of the real-time channel sounder MaMIMOSA. The upgrade consists in using RoF links to distribute the Tx antennas in different locations to emulate the distributed APs of the cell-free network in a large suburban area. Although a limited number of transmit antennas (eight) was considered, which is below the expected number in an operational distributed massive MIMO network, the study experimentally validates the promises of cell-free networks compared to co-localized antennas, with a higher and spatially more uniform SNR. The analysis of the path loss characteristics for the cell-free network also provides valuable guidelines for deploying APs in the scenario. Moreover, an important advantage of the proposed framework using MaMIMOSA lies in its high level of flexibility for the deployment of many different distributed configurations. It is also straightforwardly adaptable to include a higher number of additional APs and antennas for emulating denser cell-free networks.

VI. ACKNOWLEDGMENT

This work was supported through the CPER RITMEA project co-financed by the European Union with the European Regional Development Fund, the French state, and the Hauts-de-France Region Council.

REFERENCES

[1] E. Björnson, J. Hoydis, and L. Sanguinetti, "Massive MIMO networks: Spectral, energy, and hardware efficiency," *Foundations and Trends in Signal Processing*, vol. 11, no. 3-4, pp. 154–655, 2017.

[2] G. Interdonato, E. Björnson, H. Quoc Ngo, P. Frenger, and E. G. Larsson, "Ubiquitous cell-free massive MIMO communications," *EURASIP Journal on Wireless Communications and Networking*, vol. 2019, no. 1, pp. 1–13, 2019.

[3] Z. Chen and E. Björnson, "Channel hardening and favorable propagation in cell-free massive MIMO with stochastic geometry," *IEEE Transactions on Communications*, vol. 66, no. 11, pp. 5205–5219, 2018.

[4] J. Farah, J. Akiki, and E. P. Simon, "Energy-efficient techniques for combating the influence of reactive jamming using non-orthogonal multiple access and distributed antenna systems," in *2019 Wireless Telecommunications Symposium (WTS)*. IEEE, 2019, pp. 1–7.

[5] J. Farah, E. P. Simon, P. Laly, and G. Delbarre, "Efficient combinations of NOMA with distributed antenna systems based on channel measurements for mitigating jamming attacks," *IEEE Systems Journal*, vol. 15, no. 2, pp. 2212–2221, 2020.

[6] D. Löschenbrand, M. Hofer, L. Bernadó, S. Zelenbaba, and T. Zemen, "Towards Cell-Free Massive MIMO: A Measurement-Based Analysis," *IEEE Access*, vol. 10, pp. 89 232–89 247, 2022.

[7] T. Choi, P. Luo, A. Ramesh, and A. F. Molisch, "Co-located vs distributed vs semi-distributed MIMO: measurement-based evaluation," in *2020 54th Asilomar Conference on Signals, Systems, and Computers*. IEEE, 2020, pp. 836–841.

[8] A. P. Guevara, S. De Bast, and S. Pollin, "Weave and conquer: A measurement-based analysis of dense antenna deployments," in *ICC 2021-IEEE International Conference on Communications*. IEEE, 2021, pp. 1–6.

[9] C. Fager, S. Rimborg, E. Rådahl, H. Bao, and T. Eriksson, "Comparison of Co-located and Distributed MIMO for Indoor Wireless Communication," in *2022 IEEE Radio and Wireless Symposium (RWS)*. IEEE, 2022, pp. 83–85.

[10] P. Laly, D. P. Gaillot, M. Lienard, P. Degauque, E. Tanghe, W. Joseph, and L. Martens, "Flexible real-time mimo channel sounder for multidimensional polarimetric parameter estimation," in *2015 IEEE Conference on Antenna Measurements Applications (CAMA)*, 2015, pp. 1–3.

[11] D. Gaillot, P. Laly, N. Dahmouni, G. Delbarre, M. Van den Bossche, G. Vermeeren, E. Tanghe, E. Simon, W. Joseph, L. Martens *et al.*, "Measurement of the V2I massive radio channel with the MaMIMOSA sounder in a suburban environment," in *2021 15th European Conference on Antennas and Propagation (EuCAP)*. IEEE, 2021, pp. 1–4.

[12] P. Laly, D. P. Gaillot, G. Delbarre, M. Van den Bossche, G. Vermeeren, F. Challita, E. Tanghe, E. P. Simon, W. Joseph, L. Martens *et al.*, "Massive radio channel sounder architecture for 5G mobility scenarios: MaMIMOSA," in *14th IEEE European Conference on Antennas and Propagation (EuCAP)*, 2020, pp. 1–5.

[13] X. Zhao, J. Kivinen, P. Vainikainen, and K. Skog, "Propagation characteristics for wideband outdoor mobile communications at 5.3 ghz," *IEEE Journal on Selected Areas in Communications*, vol. 20, no. 3, pp. 507–514, 2002.